

**Electronics states of interdiffused quantum dots**

O. Gunawan

*Department of Electrical Engineering, Princeton University, Princeton, New Jersey 08544, USA*

H. S. Djie and B. S. Ooi\*

*Department of Electrical Engineering, Lehigh University, Bethlehem, Pennsylvania 18015, USA*

(Received 8 December 2004; revised manuscript received 8 March 2005; published 27 May 2005)

We have developed a three-dimensional model for electronic states calculation of interdiffused quantum dots (QDs) with arbitrary shape by solving the BenDaniel-Duke's equation in momentum space domain. The proposed model features several advantages such as automatic solution to the Fick's diffusion equation, a relatively compact and efficient Hamiltonian matrix, and natural representation of a large array of QDs. Without considering the interdiffusion effect, our model yields good agreement with our references of InAs/GaAs QDs ground state energy calculation. We analyze the interdiffusion effect in QDs with various shapes of theoretical and practical interest like spherical, cubical, pyramidal, and lens shaped. We study the effect of QD size and aspect ratio to the blueshift profile due to interdiffusion. We found a similar blueshift profile in these QDs at almost any size that can be well approximated by  $\text{sech}(x)$  function. This model will serve as a valuable tool for QD band gap engineering based on the interdiffusion technique.

DOI: 10.1103/PhysRevB.71.205319

PACS number(s): 68.65.Hb, 73.21.La, 78.67.Hc

**I. Introduction**

Semiconductor heterostructures utilizing quantum dots (QDs) and nanocrystal structure have been subjected to an extensive research field due to interest in the fundamental physics of three-dimensional quantum confinement, together with the device functionality that they can provide. Current advances in QD heterostructures on III-V compounds semiconductor have gradually placed this material system en route to succeed quantum well (QW) structure for high performance lasers, as well as other active and passive photonic components. Using the Stranski-Krastanow growth method, low threshold, high thermal stability, and high quantum efficiency lasers, and other active components have been demonstrated in In(Ga)As/GaAs QD systems.<sup>1-4</sup> The interdiffusion effect is expected to play an important role in low dimensional semiconductor structures, particularly in QDs, because of the large surface area to volume ratio compared to the bulk or QW structures. As the dimension for QDs is typically in the order of nanometers (50–500 Å), a small interdiffusion between the dots and the surrounding materials as illustrated in Fig. 1(b), is expected to produce a significant change in the band structure and the optical properties of the material.<sup>5</sup> Recently, the capability of thermal-induced interdiffusion (also referred to as intermixing or disordering)<sup>6</sup> in tailoring the shape and size and thus optical properties of self-assembled QDs (SAQDs) at postgrowth level has been applied with promising results.<sup>7-14</sup> The preservation of three-dimensional confinement in the interdiffused QDs after high temperature annealing suggests that the postgrowth control of QDs band gap via the interdiffusion technique is achievable in QD structures. The interdiffusion effect also causes sharper photoluminescence (PL) intensity indicating an improved optical property desirable for optoelectronics application. The ability to control these properties after growth offers a wide range of band gap tunability that is necessary for some device applications.<sup>16,17</sup>

In spite of numerous literatures on the interdiffusion in QWs and quantum wires, theoretical modeling of QDs interdiffusion is still lacking; mainly hampered by the complex three-dimensional nature of QDs system. Theoretical descriptions of interdiffused QD so far are limited to one<sup>15,17</sup> or two-dimensional approximation.<sup>18</sup> A simple one-dimensional model provides good approximation for thin QDs where the interdiffusion is more dominant in the thin direction. However, this model becomes inaccurate at a high degree of interdiffusion where interdiffusion is comparable in all directions. Therefore a full three-dimensional modeling of the interdiffusion effect is required to provide a more complete and versatile description of the problem.

There are several methods for solving the Schrödinger equation for QDs electronic structure calculation that mostly work in real-space domain, such as: the finite element method (discretized Schrödinger equation)<sup>19-21</sup> and the orthonormal-set expansion method.<sup>22-24</sup> In this paper, we develop an interdiffused QD model in momentum space domain. We adopt the BenDaniel-Duke's<sup>25</sup> formulation for the Schrödinger equation in momentum space and calculate the complex Fourier coefficients (FCs) of the potential functions and reciprocal effective mass to solve the Hamiltonian. Compared with the existing approaches in the real-space domain, our approach in the momentum space domain offers several advantages, such as the following.

*a. Natural representation of large arrays of QDs.* The momentum space model allows us to use periodic boundary conditions instead of a hard-wall boundary potential like in the real space model.<sup>23,24</sup> Such a boundary condition represents a periodic distribution of QDs arranged in an infinite lattice. This serves as a physically realistic model of a typical SAQD structure where QDs are grown in large numbers. Furthermore, by choosing a tetragonal lattice structure as shown Fig. 1(b), we can model two different fundamental periodicities in the SAQDs distribution. They are the periodicity of the wetting layers in vertical direction and QD den-

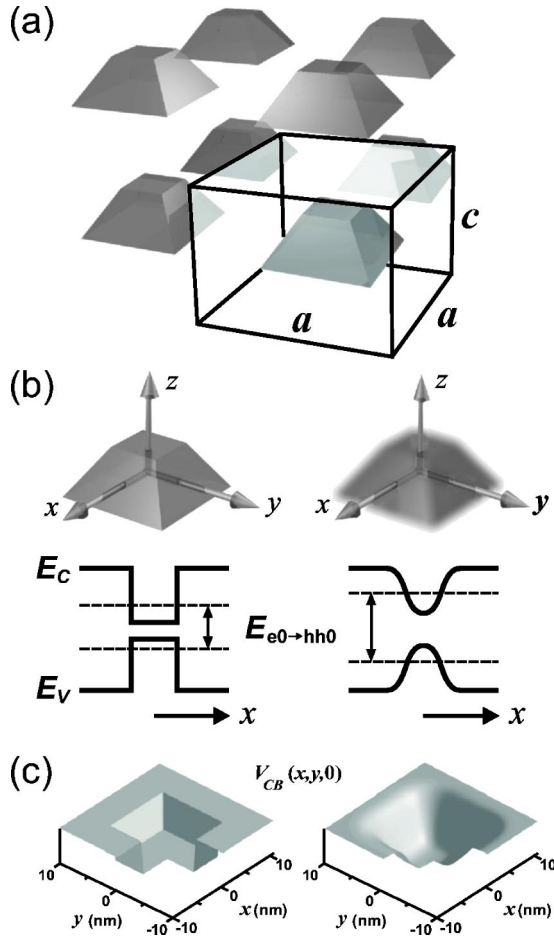


FIG. 1. (a) A superlattice of pyramidal QDs with tetragonal unit cell. (b) Interdiffusion smears the alloy distribution resulting in band gap disordering in all directions. Band gap profiles for the noninterdiffused (left) and interdiffused (right) QD along the  $x$  direction are shown. (c) Conduction band edge potential profile at  $z = 0$  plane for: noninterdiffused (left) and interdiffused (right) QD.

sities in horizontal direction. This feature is essential to model high density SAQDs, where spacing between neighboring QDs is close enough that coupling among adjacent QDs is significant. On the other hand, if the unit cell is sufficiently large compared to the QDs, the low-lying QD bound states become insensitive to the boundary conditions. As such, the model could also be used to describe an isolated QD, like the real space model with hard-wall boundary condition.

*b. Automatic solution to the Fick's diffusion equation.* One method to solve the Fick's diffusion equation is by the Fourier decomposition technique. In the reciprocal-space domain, one needs to calculate the complex FCs of the potential functions to solve the Hamiltonian. The same FCs are also used to express the solution of the Fick's diffusion equation. In general, the QD alloy concentration distribution and their related properties with approximate linear dependencies like band gap and effective mass can be calculated at any diffusion length.

*c. Small Hamiltonian matrix size and efficient matrix element computation.* A typical orthonormal-set expansion tech-

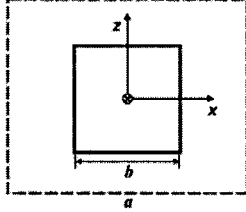
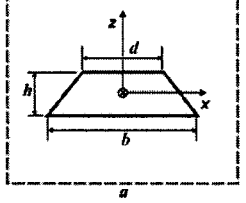
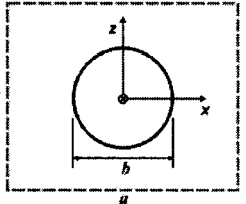
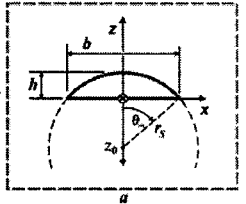
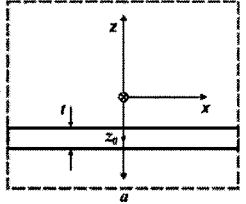
nique has small matrix size but computationally inefficient due to multiple-integration involved in calculating the matrix elements.<sup>23</sup> On the other hand, in the finite-element method or discretized Schrödinger's equation technique,<sup>19,20</sup> each matrix element can be calculated rapidly as there is no integration involved. However, the resulting Hamiltonian matrix size is very large, in the order of  $10^5 \times 10^5$ , thus computationally expensive. In contrast, the momentum space model has the best of both worlds where the matrix size is small, typically in the order of  $10^3 \times 10^3$ , and each matrix element can be computed efficiently. The only integration effort needed is to compute the FCs of the shape functions, in which some have analytical solutions. For pyramidal QD, which is a shape of great interest, analytical expression for the FCs can be used thus facilitating efficient matrix elements computation and provides intuitive clues about how the QD shape parameters will affect the result. One drawback in this model is that it requires higher order of FCs to sufficiently describe QDs with sharp feature, e.g., a pyramidal QD. Fortunately, the ground state of most QDs is not sensitive to the sharp feature of the QD, especially when they are heavily interdiffused, thus most of the computation can be done efficiently using relatively small number of FCs.

In this paper we present calculations for the case of In(Ga)As/GaAs QDs, that are of great interest and have been well investigated both theoretically and experimentally.<sup>15,17,22,23,26-28</sup> For the purpose of modeling the interdiffusion effect in three dimensions, we choose a basic single-band model for both conduction and valence band while neglecting additional effects such as strain, perturbation potential due to piezoelectricity, and multiband Hamiltonian model. Nevertheless, we utilize modified material parameters that incorporate the influence of these effects<sup>23</sup> and also account the effect of effective mass anisotropy by using the BenDaniel-Duke's formulation. Even though the model does not have the complexities that account for these additional effects, it should retain the essential physics of interdiffused QDs. We have attempted to provide a general and versatile model by investigating most common QD shapes of interest like cubical, pyramidal, spherical, and lens shaped QD. The QD shape models are characterized by their geometrical parameters like base, width, and height, therefore QDs with arbitrary size and aspect ratio can be easily defined. In general our model serves as first-order calculation that provides a framework and reference point for a more complicated treatment. It will be of great interest for experimentalists in both epitaxy growth and heterostructures intermixing communities to relate their experiments with a simple model.

## II. Quantum Dots Model

We start from noninterdiffused description of the QDs, where the QDs are distributed periodically in a tetragonal superlattice structure with dimensions:  $a \times a \times c$  as shown in Fig. 1(a). We intentionally choose tetragonal superlattice structure whose lattice constant  $a$  and  $c$  reflect two physical parameters that characterize the distribution of SAQDs in real space. First is the density of SAQDs that determines the

TABLE I. The FCs of the shape functions for the four types of QDs and a WL drawn on the  $x$ - $z$  plane of the tetragonal unit cell (see Ref. 29). The pyramidal QD described here refers to a generalized truncated pyramidal QD (see Ref. 30).

QD Shape	Complex Fourier Coefficients $c_{\mathbf{K}_{n,m,l}}$
<p><b>Cubical</b></p> 	$c_{\mathbf{K}_{n,m,l}} = \frac{b^3}{a^2 c} \operatorname{sinc}\left(\frac{b}{a} n\right) \operatorname{sinc}\left(\frac{b}{a} m\right) \operatorname{sinc}\left(\frac{b}{c} l\right)$ $\operatorname{sinc}(x) = \frac{\sin \pi x}{\pi x}$ $V_{QD} = b^3$
<p><b>Pyramidal</b></p> 	$c_{\mathbf{K}_{n,m,l}} = \frac{e^{-i2\pi \frac{z_0}{c} l}}{2\pi^3 m n} \left( \frac{\cos\left[\pi(m+n)(\alpha z + \beta)/a - i \tanh^{-1}[\alpha(m+n)a/2lc]\right]}{\sqrt{[\alpha(m+n)c/a]^2 - (2l)^2}} \right. \\ \left. \frac{\cos\left[\pi(m-n)(\alpha z + \beta)/a - i \tanh^{-1}[\alpha(m-n)a/2lc]\right]}{\sqrt{[\alpha(m-n)c/a]^2 - (2l)^2}} \right) \Bigg _{z=-h/2}^{z=h/2}$ $\alpha = (d-b)/h \quad \beta = (d+b)/2$ $V_{QD} = \frac{1}{3}[(b^2 + d^2)h + hbd]$
<p><b>Spherical</b></p> 	$c_{\mathbf{K}_{n,m,l}} = \frac{1}{a^2 c} \int_0^{2\pi} \int_0^{\pi} \left( \frac{e^{-ik_{\theta\phi} r} (-2i + 2k_{\theta\phi} r + ik_{\theta\phi}^2 r^2)}{k_{\theta\phi}^3} \right) \Bigg _{r=0}^{r=b/2} \sin \theta d\theta d\phi$ $k_{\theta\phi} = \frac{2\pi}{a} (n \sin \theta \cos \phi + m \sin \theta \sin \phi) + \frac{2\pi}{c} l \cos \theta$ $V_{QD} = \frac{1}{6} \pi b^3$
<p><b>Lens-Shaped</b></p> 	$c_{\mathbf{K}_{n,m,l}} = \frac{e^{-i2\pi \frac{z_0}{c} l}}{a^2 c} \int_0^{2\pi} \int_0^{\theta_m} \left( \frac{e^{-ik_{\theta\phi} r} (-2i + 2k_{\theta\phi} r + ik_{\theta\phi}^2 r^2)}{k_{\theta\phi}^3} \right) \Bigg _{r=r_0}^{r=r_s} \sin \theta d\theta d\phi$ $k_{\theta\phi} = \frac{2\pi}{a} (n \sin \theta \cos \phi + m \sin \theta \sin \phi) + \frac{2\pi}{c} l \cos \theta$ $r_s = (4h^2 + b^2)/8h \quad r_0 = (r_s - h) \sec \theta \quad \theta_m = \arccos(1 - h/r_s)$ $V_{QD} = \frac{1}{24} \pi h (4h^2 + 3b^2)$
<p><b>Wetting Layer</b></p> 	$c_{\mathbf{K}_{n,m,l}} = e^{-i2\pi \frac{z_0}{c} l} \delta_{n,m,0} \frac{t}{c} \operatorname{sinc}\left(\frac{t}{c} l\right)$

average spacing ( $a$ ) between QDs in the horizontal ( $x$ - $y$ ) plane. Second is the period of the wetting layer that governs the periodicity of the SAQDs ( $c$ ) in the growth direction ( $z$ ). Clearly, the model will reduce to simple lattice structure for  $c=a$ . On the other hand, for most SAQDs system the spacing between adjacent QDs are very large, therefore the QDs appear as an isolated QDs. In this regime we can limit the relative size of the unit cell so that accurate result still can be obtained with a finite number of FCs in the calculation. In this case a tetragonal lattice model is essential for efficient calculation, as often times the QDs have a very low aspect

ratio ( $h/b$ ) and one can adjust the size of the lattice constant  $a$  and  $c$  accordingly.

The three-dimensional band edge potential and the carrier effective mass depend on the alloy concentration at every point in space that are essentially determined by the shape of the QD in the three dimensions. For that purpose, we define a shape function within a unit cell

$$f_{QD}(\mathbf{r}) = \begin{cases} 1 & \text{inside QD} \\ 0 & \text{outside QD} \end{cases} \quad (1)$$

For example, using the shape function, the band-edge potential function can be expressed as:  $V_B(\mathbf{r}) = V_{B0} f_{QD}(\mathbf{r})$ , where the subscript  $B$  represents either conduction or valence band edge.  $V_{B0}$  has a negative value to represent potential confinement inside the QD.

Since the shape function is periodic in space, we can express it in terms of complex Fourier series

$$f_{QD}(\mathbf{r}) = \sum_{\mathbf{K}} c_{\mathbf{K}} e^{i\mathbf{K}\cdot\mathbf{r}}, \quad (2)$$

where  $\mathbf{K}$  is the reciprocal lattice vector that runs through all lattice points. For tetragonal lattice it is defined as

$$\mathbf{K}_{n,m,l} = 2\pi/a[n\hat{\mathbf{x}} + m\hat{\mathbf{y}}] + 2\pi/l\hat{\mathbf{z}} \quad (3)$$

with  $n$ ,  $m$ , and  $l$  are integers running from  $-\infty$  to  $\infty$ . Occasionally these subscripts are omitted for convenience.

The complex FCs have to be calculated by performing the required integration within a unit cell. By definition of the shape function in Eq. (1), the integration only prevails inside the QD that allows a great simplification

$$c_{\mathbf{K}} = \frac{1}{a^2c} \int_{\text{unit cell}} f_{QD}(\mathbf{r}) e^{-i\mathbf{K}\cdot\mathbf{r}} d\mathbf{r} = \frac{1}{a^2c} \int_{QD} e^{-i\mathbf{K}\cdot\mathbf{r}} d\mathbf{r}. \quad (4)$$

It is desirable to obtain the analytical expression of the FCs in Eq. (4) to optimize computational speed and accuracy and more importantly to give a physical insight of how various QD geometrical parameters will affect the calculation. Table I presents the result of our calculation for several QD shapes of great interest: cubical, pyramidal, spherical, and lens shaped. For QDs with rectangular symmetry such as cubical and pyramidal QDs analytical expressions can be derived. However, for spherical and lens-shaped QDs that possess spherical symmetry, only semianalytical expressions can be obtained where subsequent numerical integrations are required.

All QD shape functions have to be real functions, therefore the following property applies:  $c_{-\mathbf{K}} = c_{\mathbf{K}}^*$ . This fact is useful in numerical computation such as for the spherical and lens-shaped QD, so that only half of the spectrum need to be calculated. Another noteworthy property is that the volume of the QD is equal to product of zeroth order FC and the volume of the unit cell ( $V_{QD} = c_{\mathbf{K}_{0,0,0}} a^2c$ ). In other words,  $c_{\mathbf{K}_{0,0,0}}$  can also be viewed as the average of the QD material in the unit cell.

For completeness, a special shape function called wetting layer (WL) is presented in Table I to construct composite QD model by exploiting the linear property of Fourier transform. A real SAQD system such as QDs grown on WLs can be represented as a superposition of QDs and WLs. The superposition applies to the shape function as well as to the FCs. So in this example, the FC of the composite QD can be simply expressed as

$$c_{\mathbf{K},QD+WL} = c_{\mathbf{K},QD} + c_{\mathbf{K},WL}. \quad (5)$$

However, there is a caveat, each shape function must not overlap with each other for Eq. (5) to hold. This is a consequence of the way we define QD shape function in Eq. (1).

A typical WL is very thin with respect to the average lattice spacing  $a$  or  $c$ ,<sup>31</sup> thus higher order of FCs ( $N_{FC}$ ) are required to sufficiently represent its potential function. A rule of thumb following ‘‘Nyquist’’ criteria is that we should choose  $N_{FC} > c/t$ , where  $c$  is the vertical lattice constant and  $t$  is the WL thickness. This is generally true for any QDs as well, where the thickness  $t$  represents the critical dimension (usually the thinnest dimension) that affects the energy levels the most. If the WL is very thin relative to the size of QD one could safely neglect it. This is especially true when there is interdiffusion, as a thin WL will be more quickly interdiffused compared to the QD.<sup>32</sup> For this reason we normally neglect any presence of a WL in our calculation presented here, however, one may be interested to model the WL, for example to study the coupling between the quantum states in the WL and QD.

Another useful property of the Fourier transformation for constructing a composite QD model is the shift theorem. A translation in real-space domain by a vector  $\mathbf{r}_0$ , is simply reflected by a multiplication of  $\exp(-i\mathbf{K}_{n,m,l}\cdot\mathbf{r}_0)$  to the FCs. For example the FC of the WL has a factor of  $\exp(-i2\pi lz_0/c)$  that reflects a shift of the WL center to coordinate  $z_0$  on the  $z$  axis. This is used to position the WL just underneath the QD. Similarly, the lens-shaped QD is shifted so that the center of the imaginary sphere is located at  $z_0$ , to conveniently position the QD in the center of the unit cell and ensure that the whole QD is contained within the unit cell.

### III. The Hamiltonian Model

To calculate the bound energy levels and the wave function for the electron and holes we use the single-band effective-mass approximation to the Schrödinger’s equation. In the framework of envelope function scheme and effective mass approximation, the Schrödinger’s equation in BenDaniel-Duke’s<sup>25</sup> formulation is given as

$$-\frac{\hbar^2}{2} \nabla \cdot \left[ \frac{1}{m^*(\mathbf{r})} \nabla \Psi(\mathbf{r}) \right] + V(\mathbf{r})\Psi(\mathbf{r}) = E\Psi(\mathbf{r}). \quad (6)$$

In semiconductor heterostructures, especially for interdiffused heterostructures, the nonuniform distribution of the alloy concentration results in anisotropic distribution of effective mass of the carriers. The BenDaniel-Duke’s equation formulation ensures that the carrier’s probability current is conserved throughout the space.

In a periodic potential, the solution of the Schrödinger’s equation eigenwave functions can be written as

$$\Psi_{\mathbf{k}}(\mathbf{r}) = \sum_{\mathbf{K}} C_{\mathbf{k}+\mathbf{K}} e^{i(\mathbf{k}+\mathbf{K})\cdot\mathbf{r}}, \quad (7)$$

where  $\mathbf{k}$  is crystal momentum of the carrier. This form of solution ensures that the Bloch’s theorem is satisfied.

We then transform the real space BenDaniel-Duke’s equation into momentum space (or reciprocal space) domain, whose derivation is presented in the Appendix



$$\sum_{\mathbf{K}'} \left\{ \frac{\hbar^2}{2} M_{\mathbf{K}-\mathbf{K}'} [(\mathbf{k} + \mathbf{K}')^2 + (\mathbf{K} - \mathbf{K}') \cdot (\mathbf{k} + \mathbf{K}')] - \delta_{\mathbf{K}-\mathbf{K}'} E + U_{\mathbf{K}-\mathbf{K}'} \right\} C_{\mathbf{k}+\mathbf{K}'} = 0, \quad (8)$$

where  $\delta_{\mathbf{K}-\mathbf{K}'}$  is the Kronecker delta function, with  $\delta_{\mathbf{K}-\mathbf{K}'} = 1$  for  $\mathbf{K} = \mathbf{K}'$  and 0 otherwise.  $M_{\mathbf{K}}$  is the FC of the reciprocal effective mass,  $U_{\mathbf{K}}$  is the FC of the potential function in the conduction or valence band edge. While  $E$  is the eigenenergy and  $C_{\mathbf{K}}$  is the FC of the eigenwave functions. Equation (8) above is the secular equation of the Hamiltonian that facilitates a rather straight forward programming effort to compute the eigenenergies and wave functions. For our purpose in this paper, we calculate the bound energy levels at  $\mathbf{k} = 0$  that represents the  $\Gamma$  point of the QD superlattices Brillouin zone. In principle one could derive the multiband version of the Hamiltonian in momentum space akin to Eq. (8), to give more realistic description of the valence band states. However, in order to focus our study on the three-dimensional interdiffusion effect, a single-band Hamiltonian model should be sufficient.

#### IV. Interdiffusion Model

We present the standard model of interdiffusion in binary alloy based on simplifying assumption of linear and isotropic diffusion process. The position-dependent function of the fractional alloy concentration  $x(\mathbf{r})$  is related to the shape function as defined in Eq. (1):

$$x(\mathbf{r}) = x_B + (x_W - x_B) f_{QD}(\mathbf{r}), \quad (9)$$

where  $x_W$  is the initial alloy concentration inside the QD (well) region and  $x_B$  outside the QD (barrier) region.

Consider an isotropic interdiffusion process, that can be described by Fick's law

$$\frac{\partial x(\mathbf{r})}{\partial(Dt)} = \nabla^2 x(\mathbf{r}), \quad (10)$$

where  $Dt = L_d^2$ , with  $D$  is the diffusion constant,  $t$  is diffusion time, and  $L_d$  is the diffusion length. This equation is a linear second order partial differential equation, therefore quantities linearly related to  $x(\mathbf{r})$  should also obey the same equation and have similar solution. The Fick's diffusion equation can be solved by Fourier decomposition technique, whose solutions can be expressed as

$$x(\mathbf{r}, L_d) = \sum_{\mathbf{K}} (u_{\mathbf{K}} e^{-\mathbf{K}^2 L_d^2}) e^{i\mathbf{K} \cdot \mathbf{r}}. \quad (11)$$

In other words, upon interdiffusion, the FCs are attenuated by a factor of  $\exp(-\mathbf{K}^2 L_d^2)$ :

$$u_{\mathbf{K}}(L_d) = u_{\mathbf{K}} e^{-\mathbf{K}^2 L_d^2}. \quad (12)$$

This is a useful relationship, as it applies to FCs of any quantities that are linearly related to  $x$ , including the shape function whose FCs is  $c_{\mathbf{K}}$ .

Using Vegard's law, the band gap of most III-V heterostructures can be approximated as a linear interpolation of the fractional alloy concentration

$$E_g(x) = a_E + b_E x, \quad (13)$$

where  $x$  is the fractional concentration of a III-V element  $A_x B_{1-x}$ . Here we can express the potential confinement in conduction or valence band as

$$V_B(\mathbf{r}) = Q_B [E_g(\mathbf{r}) - E_{gB}], \quad (14)$$

where  $E_{gB} = a_E + b_E x_B$  is the band gap at the barrier that serves as the zero reference, and  $Q_B$  is the band offset coefficient. Combining with Eq. (9), the FCs of this potential function can be readily expressed as a function of the shape functions FC ( $c_{\mathbf{K}}$ ):

$$U_{B,\mathbf{K}} = Q_B b_E (x_W - x_B) c_{\mathbf{K}}. \quad (15)$$

Alternatively, one could substitute  $Q_B b_E$  with the potential depth inside the QD ( $V_{0e}$  or  $V_{0hh}$ ) if it is known. The effective mass of electron in most III-V heterostructures can also be written in terms of linear interpolation of the alloy concentration  $x$ . However, it is the reciprocal effective mass term ( $M_{\mathbf{K}}$ ) that is needed to construct the secular Hamiltonian matrix [Eq. (8)]. In the spirit of Vegard's law we apply the same interpolation method for the reciprocal effective mass

$$\frac{1}{m^*} = a_M + b_M x. \quad (16)$$

Combining this with Eq. (9) we can readily express the FCs of the reciprocal effective mass as a function of the shape function's FC ( $c_{\mathbf{K}}$ ):

$$M_{\mathbf{K}} = (a_M + b_M x_B) \delta_{\mathbf{K}} + b_M (x_W - x_B) c_{\mathbf{K}}. \quad (17)$$

From Eqs. (15) and (17), the use of a separate shape function  $f_{QD}$  and its FCs are clearly justified, as four sets of quantities namely  $U_{B,K}$  and  $M_{\mathbf{K}}$  for both conduction and valence band, all can be expressed as simple linear functions of  $c_{\mathbf{K}}$ .

Following Eq. (12), the effect of interdiffusion to the potential function and the reciprocal effective mass are simply reflected as an attenuation to their FCs by factor  $\exp(-\mathbf{K}^2 L_d^2)$ ,

$$U_{\mathbf{K}}(L_d) = U_{\mathbf{K}} e^{-\mathbf{K}^2 L_d^2}, \quad (18)$$

$$M_{\mathbf{K}}(L_d) = M_{\mathbf{K}} e^{-\mathbf{K}^2 L_d^2}. \quad (19)$$

This fact highlights our main motivation working in momentum space domain, as the solution to the Fick's diffusion equation comes automatically. Figure 1(c) presents a two-dimensional cross section of the conduction band's potential function for a noninterdiffused and an interdiffused QD.

Although in real QD structures such as in InAs/GaAs QD, the presence of strain is significant, there has been no consensus about to what extent the strain influences the interdiffusion. Ryu *et al.*<sup>33</sup> proposed a non-Fickian diffusion model that takes into account the effect of strain in InGaAs/GaAs heterostructure. However, in similar experiment using two multiple QWs of InGaAs/GaAs with four sets of different Indium concentration each, Gillin<sup>34</sup> observed no effect of the strain on the interdiffusion process. If the strain fields within the QDs are quite uniform, we can rea-

sonably assume that the diffusion process is approximately isotropic.

### V. Computation

In this section, we present calculations for InAs/GaAs QDs system. We use the material parameters set as used in Ref. 23 where a single band Hamiltonian with constant confining potential model is used. For electron we have:  $V_{0e} = 450$  meV, InAs  $m_e^* = 0.04 m_e$ , GaAs  $m_e^* = 0.0665 m_e$ . For heavy hole we have:  $V_{0hh} = 266$  meV, InAs  $m_{hh}^* = 0.59 m_e$ , GaAs  $m_{hh}^* = 0.377 m_e$ . We neglect the presence of any WL in our calculation.

To construct the secular matrix equation [Eq. (8)] we need to calculate the FCs for the potential and the reciprocal effective mass whose index  $\mathbf{K}$  has subindexes  $n, m, l$  running from  $-N_{FC} \dots N_{FC}$  each. The resulting secular matrix has a total size  $(2N_{FC}+1)^3 \times (2N_{FC}+1)^3$ . However, due to the convolution in the  $\mathbf{K}$  index in both  $M_{\mathbf{K}-\mathbf{K}'}$  and  $U_{\mathbf{K}-\mathbf{K}'}$  in Eq. (8), FCs up to the order of  $2N_{FC}$  are taken into account, which actually works to our advantage. MATLAB is used as the programming platform. It has an eigenvalue solver function based on the ARPACK routine capable of solving large few eigenvalue problem. Further reduction in matrix size is possible by exploiting the symmetry of the QD such as the pyramidal and cubic QD that belong to  $C_{4v}$  symmetry group.

The critical parameters to yield an accurate bound state calculation are the number of maximum order of FCs ( $N_{FC}$ ) and the relative size of unit cell with respect to QDs size ( $a/b$ ) which basically determines the boundary condition. Figure 2 shows the electron ground state energies at varying  $a/b$  values calculated with different  $N_{FC}$ . The calculation is done for a noninterdiffused InAs/GaAs cubical and pyramidal QDs with the same volume. As we increase the order of FCs ( $N_{FC}$ ) involved in the calculation, the curves converge to their asymptotic limit (shown as dotted line labeled  $N_{FC} = \infty$ ). However, as we bring all QDs closer ( $a/b < 2$ ), the ground state energy decreases as the coupling between neighboring QDs becomes stronger due to increased tunneling. We notice that for pyramidal QDs, the convergence is slower than the cubic QD. This is due to the sharp feature in the apex of the pyramid that requires higher order of Fourier components to sufficiently describe it. A typical parameter we use are  $N_{FC} = 5$  and  $a/b \approx 3$  to obtain sufficiently accurate results with convergence error not more than 5%. Similar situations apply in choosing the value of the vertical tetragonal lattice size ( $c$ ). In this case, we also use  $c/h \approx 3$  to maintain sufficiently accurate result.

Before investigating the interdiffusion effect in QDs, it is instructive to validate our model against others' works in calculating noninterdiffused QDs bound states. In our model, a noninterdiffused QDs is simply described by setting  $L_d = 0$ . For the case of InAs/GaAs pyramidal QD, Cusack *et al.*<sup>26</sup> and Grundmann *et al.*<sup>27</sup> have calculated the bound states electron energies using a considerably detailed model incorporating strain and piezoelectric effect. The calculations were performed at varying size of pyramidal QD with a fixed aspect ratio  $h/b = 0.5$ . The range of size from  $b = 60$  to  $200$  Å, represents a range of typical pyramidal QDs size found in

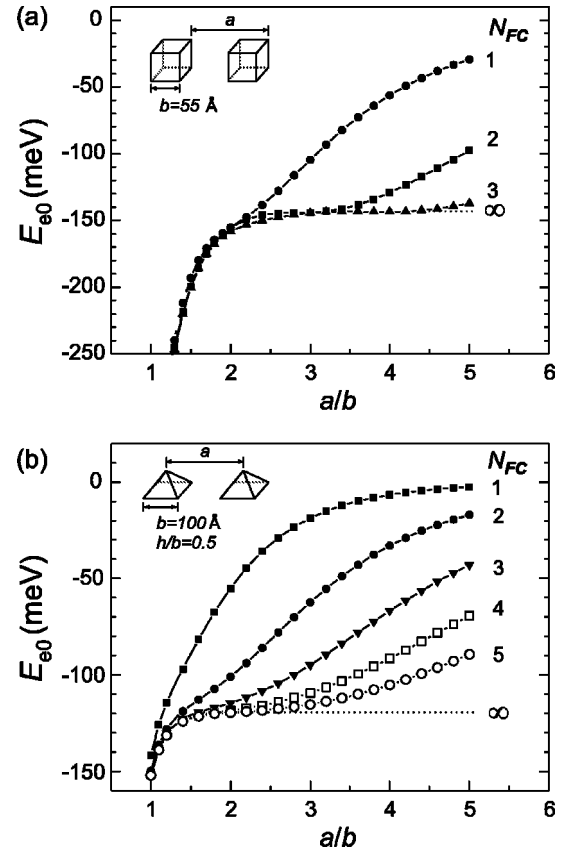


FIG. 2. Convergence of electron ground state energies at increasing  $N_{FC}$  and as a function of  $a/b$  for: (a) cubical QD, (b) pyramidal QD. Both QDs have the same volume and unit cell. The dotted line indicates asymptotic curve for  $N_{FC} = \infty$ .

practice. Using the material parameters as used by Califano *et al.*,<sup>23</sup> we reproduce the results (solid curve) as shown in Fig. 3. In general, our calculation fall within 12% of the more complicated calculation results of Cusack *et al.* and Grundmann *et al.*, a reasonable result considering many simplifications we made in our model.

### VI. Results and Discussion

Besides material parameters that one has less control with, a QD have additional parameters such as the shape, size, and aspect ratio (if applicable) that uniquely describe it. In this section we will study the interdiffusion effect to the QD ground state energy levels and particularly the effect of QD shape and size.

Figure 4 presents our calculation for the ground state transition energies ( $E_{e0 \rightarrow hh0}$ ) on four different shapes of iso-volume QDs at increasing degree of interdiffusion represented by the diffusion length ( $L_d$ ). In general we observe the well known effect of interdiffusion on quantum heterostructures, i.e., blueshifting of the energy levels. Despite having the same volume, the ground energies are different, from lowest to highest: spherical, cubical, lens-shaped, and pyramidal QD. This difference is attributed to increasing presence of sharp feature in those QDs. The carrier wave function tends

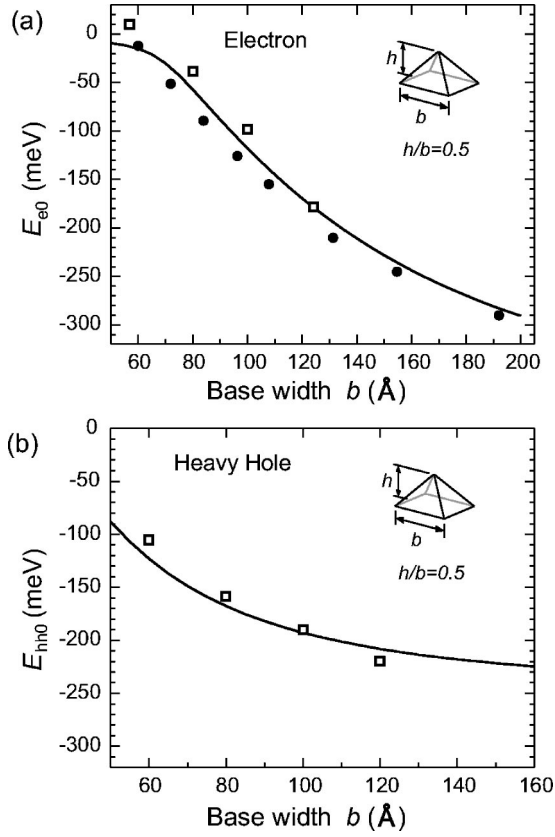


FIG. 3. Validation of our model (solid line) for noninterdiffused InAs/GaAs pyramidal QDs with the theoretical models from Cusack *et al.* (hollow squares) and Grundmann *et al.* (filled circles). The plots display ground state energies with respect to the unstrained GaAs conduction and valence band, respectively, for (a) electron and (b) heavy holes.

not to occupy the sharp corners, making the effective size of the QD is smaller leading to a higher bound state energy. For the practical application of QD band gap engineering via interdiffusion technique, one would like to achieve the largest blueshift range possible. Therefore, sharp features and small aspect ratio in QD shape are undesirable. In this respect, lens shaped QD are preferred over pyramidal QDs.

In Fig. 4, at very high diffusion length all ground state energies converge to the same value. This situation represents a completely interdiffused system, where the QDs have lost confinement and their energy levels merge to the barrier's continuum energy levels. From the point of view of our model, this can be understood from the fact that at very high diffusion length all components of FCs [Eq. (18)] are completely attenuated except the zeroth order component ( $c_{\mathbf{K}_{0,0,0}}$ ). Thus since all the QDs and their unit cells have the same volume (same  $c_{\mathbf{K}_{0,0,0}}$ ), their ground state energies converge to  $E_{e0 \rightarrow hh0} = c_{\mathbf{K}_{0,0,0}}(V_{0e} + V_{0hh})$  at very high diffusion length.

Despite difference in shapes, all the QDs here show qualitatively similar blueshift characteristics. This similarity suggests that an empirical equation can be used to describe this common behavior. Indeed we found that if we normalize the blue shift curves, they fit reasonably well to  $\text{sech}(x)$  function.

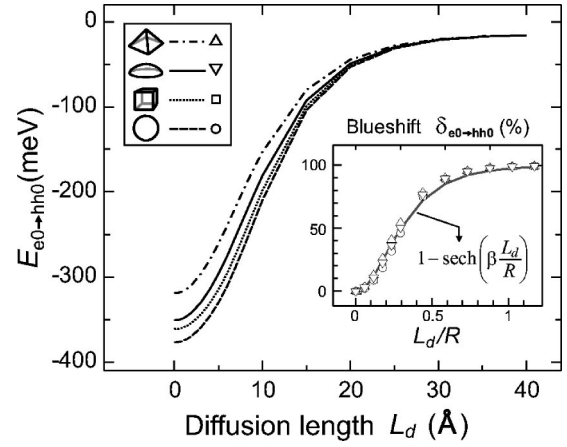


FIG. 4. The interdiffusion effect on the ground state transitional energies for the four types of isovolume QDs ( $V_{QD} = 167 \times 10^3 \text{ \AA}^3$ ) with the same unit cell. The lens-shaped and pyramidal QD have aspect ratio  $h/b = 0.5$  (Inset: Normalized blueshift that follows an empirical  $\text{sech}(x)$  curve.

Here 0% blueshift correspond to ground state transition energy ( $E_{e0 \rightarrow hh0}$ ) of noninterdiffused QD ( $L_d = 0$ ) and 100% to a completely interdiffused QD ( $L_d \rightarrow \infty$ ). A very interesting and important feature of this empirical model is that there is only one independent parameter, we call blueshift rate coefficient (BRC) designated as  $\beta$ , that characterizes the blueshift profile. This parameter  $\beta$  actually represents the rate of interdiffusion where a higher  $\beta$  corresponds to a higher interdiffusion rate. We can write this empirical model as

$$\delta_{e0 \rightarrow hh0} = \frac{\Delta E_{e0 \rightarrow hh0}}{E_{e0 \rightarrow hh0}} = 1 - \text{sech}\left(\beta \frac{L_d}{R}\right), \quad (20)$$

where  $\delta_{e0 \rightarrow hh0}$  is the normalized transitional ground state energy blueshift and  $R$  represents the size of the QD, which is the radius of a spherical QD of the same volume, given as  $R = \sqrt[3]{4V_{QD}/3\pi}$ .<sup>35</sup> The inset in Fig. 4 shows the  $\text{sech}(x)$  curve that fits well to the data points of the normalized energy blueshifts for the four types of QDs.

We are now interested in how the size and aspect ratio (for lens-shaped and pyramidal QD) influence the blueshift characteristics. We calculate the blueshift interdiffusion profile ( $E_{e0 \rightarrow hh0}$  vs  $L_d$ ) such as the one in Fig. 4 and repeat them at various  $R$  for all type of QDs. Then we inspect whether they fit to the  $\text{sech}(x)$  curve. If they do, we extract the parameter  $\beta$  using a standard curve-fitting procedure. The result is presented in Fig. 5.

We found that the blueshift interdiffusion profile fits to the  $\text{sech}(x)$  model in almost entire range of QD size, with exception of very small QDs ( $R < 20 \text{ \AA}$ ). Figure 5 shows a striking feature, for any given QD size, all QDs have practically the same parameter  $\beta$ , indicating that the interdiffusion rate is not sensitive to the shape, but rather it is more sensitive to the size of the QD. The size dependence becomes stronger for smaller QDs where the quantum confinement becomes more significant. In this regime we have  $R < \lambda_{ve}$  and  $R < \lambda_{vhh}$  where  $\lambda_{ve} = h/\sqrt{2m_e^*V_{0e}}$  and  $\lambda_{vhh} = h/\sqrt{2m_{hh}^*V_{0hh}}$ , the de-Broglie wavelength of the carri-

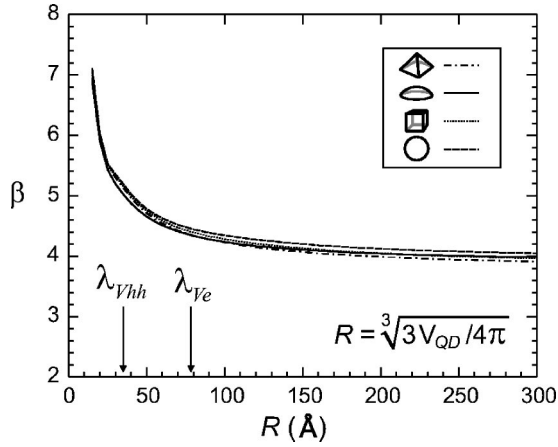


FIG. 5. Variation of  $\beta$  with respect to the QD size  $R$  for the four types of QDs. The lens-shaped and pyramidal QD have aspect ratio  $h/b=0.5$ . The volume ratio of the QD to the unit cell are kept constant (constant  $c_{\mathbf{k}_{0,0,0}}$ ).

ers having kinetic energy equal to the potential height of the QDs. Here the smaller size of QD also leads to higher ground state energies. This fact implies that small QDs are not favorable for QD band gap engineering, first because the ground state energy levels are higher causing smaller range of blueshift tunability, second because the interdiffusion rate is higher and very sensitive to the size, rendering interdiffusion control more difficult. In another aspect, for these small QDs since there is a strong dependence for the blueshift rate ( $\beta$ ) with respect to QD size as shown in Fig. 5, it is possible to deduce the size of the QDs from its blueshift profile using interdiffusion experiment. This provides an interesting application of interdiffusion technique as an alternative for QD size determination.

Besides the size of QD, lens-shaped and pyramidal QD have another critical parameter which is the aspect ratio ( $h/b$ ). Figure 6(a) shows blueshift profiles of lens-shaped QDs with varying aspect ratio but constant volume (and also fixed unit cell's volume). The blueshift interdiffusion profiles for aspect ratio  $h/b=0.5$  down to  $h/b=0.3$  still follow the  $\text{sech}(x)$  model. However, for a smaller aspect ratio ( $h/b \leq 0.2$ ), that represents very thin QDs, significant deviation appears so that they no longer fit to the  $\text{sech}(x)$  curves. This fact indicates a limitation to the model. Apparently for very thin QDs, initial interdiffusion occurs more dominant in one direction, rendering them essentially as a one-dimensional interdiffusion system instead of three-dimensional one. As the interdiffusion proceeds, interdiffusion in other directions become comparable. This transition from one-dimensional to three-dimensional interdiffusion in thin QDs appears as a kink in the blueshift curve indicated by an arrow in Fig. 6(a).

For lens QD with a higher aspect ratio ( $h/b \geq 0.3$ ),<sup>36</sup> the  $\text{sech}(x)$  model still applies and the parameter  $\beta$  is presented in Fig. 6(b), which is essentially no different with Fig. 5. However, for the aspect ratio  $h/b=0.3$ , we notice a small deviation starts to develop at small  $R$ . We note that the results presented on lens-shaped QDs here also apply to the truncated pyramid QDs.

Finally we would like to apply our model to study an experimental result of interdiffused lens-shaped InAs/GaAs

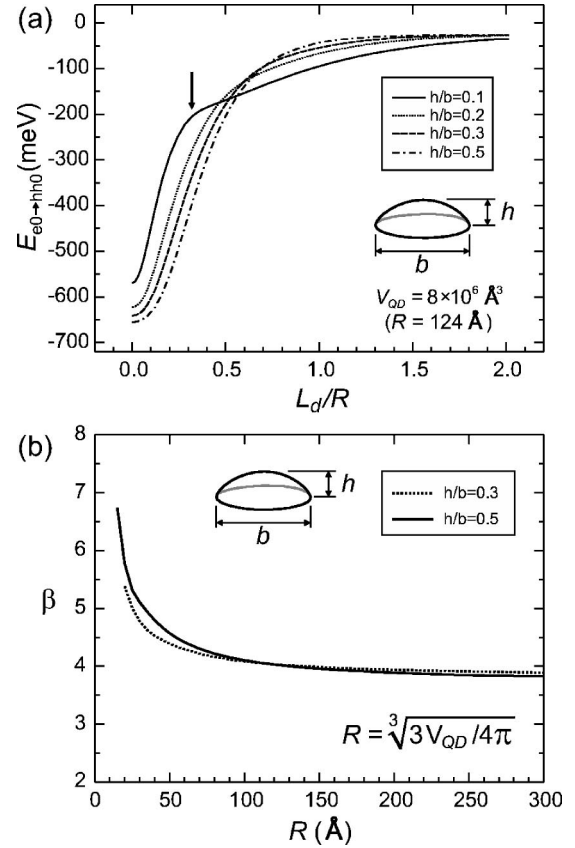


FIG. 6. (a) Blueshift profile of isovolume lens shaped QDs with varying aspect ratio. The profile for thin lens QDs with aspect ratio  $h/b \leq 0.2$  do not fit to  $\text{sech}(x)$  curve anymore and exhibits a kink indicated by an arrow (see text). (b) Lens-shaped QDs  $\beta$  parameter at various size and aspect ratio.

QD done by Fafard *et al.*<sup>15</sup> This experimental result is chosen for the availability of the diffusion lengths data deduced from the WL blueshift thus allowing a direct comparison with our model. Using standard rapid thermal annealing technique, the interdiffused QD's achieved significant blueshifts up to 200 meV. Reference 15 presents PL data that exhibit the expected blueshifts behavior and indicates a typical aspect ratio of the QDs to be  $h/b=1/8$ , however, the size of the QD for the sample presented (sample D)<sup>15</sup> is not known. Since the aspect ratio is small we can not use the  $\text{sech}(x)$  empirical model described above, so we have to resort to full calculation using our model. From the ground state transitional energy ( $E_{e0 \rightarrow hh0}$ ) PL peak, we deduced the base diameter of the QD to be  $b=(195 \pm 20)$  Å, given the aspect ratio  $h/b=1/8$ . About 10% uncertainty in  $b$  comes from the fact that our model is only that much accurate compared to more sophisticated models discussed in Sec. V. We neglect the presence of the WL for the reason mentioned in Ref. 32. Then we calculate the blueshift interdiffusion characteristics shown as a solid curve in Fig. 7. The gray band is the range of possible blueshift profiles given  $\pm 10\%$  uncertainty of  $b$ . Our model shows a reasonably good agreement with the experimental data (circles). This result demonstrates that our model provides a good description for the QD interdiffusion problem despite a number of simplifications and



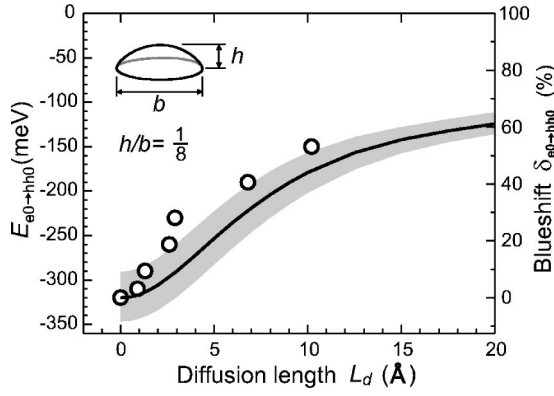


FIG. 7. Comparison of experimental data (circles) of interdiffused InAs/GaAs lens-shaped QDs from Ref. 15 and our calculation (solid curve) and its uncertainties (gray band). The diffusion lengths on the horizontal axis are deduced from the blueshift of the WL.

approximations made in our model. A closer inspection shows a higher blueshift compared to the theoretical values. Even though this discrepancy can be attributed to the inaccuracies of our model, we cannot rule out the fact that there may be some initial interdiffusion already present that was induced during sample growth at an elevated temperature.<sup>15</sup> A finite initial diffusion length will shift the experimental data points (circle) to the right, in better agreement with the theoretical curve.

## VII. Conclusions

In this paper, we present an approach to analyze the electronic structure of interdiffused quantum dots by solving the BenDaniel-Duke's equation in the momentum space. This approach offers some advantages such as automatic solution to the diffusion equation, reduction in the Hamiltonian matrix size and natural representation of large arrays of QDs. Four types of QDs model namely cubical, spherical, pyramidal, and lens shaped were developed. The interdiffusion effects on the energy levels of these QDs have been analyzed and some similarities in the blueshift profiles have been observed. Based on this observation we propose a simple empirical model using  $\text{sech}(x)$  function to estimate the blueshift profile based on a single parameter  $\beta$  that characterize the rate of interdiffusion. This model applies to QDs of any shape and any size where the confinement in all three dimensions are comparable, such as spherical QD, cubic QD, and also lens-shaped and pyramidal QDs with aspect ratio  $h/b \geq 0.3$ . We found that smaller QDs not only have a smaller range of blueshift tunability but also a higher interdiffusion rate rendering them less desirable for application utilizing QD interdiffusion. We also have related our model to an experimental data and found a good agreement. The model presented here will serve as a valuable tool for QD band gap engineering based on the interdiffusion technique.

## ACKNOWLEDGMENTS

Part of this work was performed at the Nanyang Technological University Singapore. The authors would like to

thank Professor Mansour Shayegan, Professor Stephen Lyon of Princeton University, and Dr. Wirawan Purwanto of The College of William and Mary for support and illuminating discussion.

## Appendix

Here we derive the secular equation of the Hamiltonian for the BenDaniel-Duke's formulation in momentum space domain. Starting from the Schrödinger's equation in the envelope-function scheme and effective-mass approximation

$$-\frac{\hbar^2}{2} \nabla \cdot \left[ \frac{1}{m^*(\mathbf{r})} \nabla \Psi(\mathbf{r}) \right] + V(\mathbf{r})\Psi(\mathbf{r}) = E\Psi(\mathbf{r}). \quad (\text{A1})$$

Using the identity  $\nabla \cdot (\phi \mathbf{A}) = (\nabla \phi) \cdot \mathbf{A} + \phi \nabla \cdot \mathbf{A}$ :

$$-\frac{\hbar^2}{2} \left[ \frac{1}{m^*(\mathbf{r})} \nabla^2 \Psi(\mathbf{r}) + \nabla \cdot \frac{1}{m^*(\mathbf{r})} \cdot \nabla \Psi(\mathbf{r}) \right] + V(\mathbf{r})\Psi(\mathbf{r}) = E\Psi(\mathbf{r}). \quad (\text{A2})$$

Since the potential function is periodic, the eigenwave functions should satisfy the Bloch's theorem  $\Psi(\mathbf{r}) = u_{\mathbf{k}}(\mathbf{r})e^{i\mathbf{k}\cdot\mathbf{r}}$ , where for every wave function having crystal momentum  $\mathbf{k}$  it can be expanded in terms of reciprocal lattice vector  $\mathbf{K}$ :

$$\Psi(\mathbf{r}) = \sum_{\mathbf{K}} C_{\mathbf{k}+\mathbf{K}} e^{i(\mathbf{k}+\mathbf{K})\cdot\mathbf{r}} = \sum_{\mathbf{q}} C_{\mathbf{q}} e^{i\mathbf{q}\cdot\mathbf{r}}. \quad (\text{A3})$$

The potential function can also be expressed in terms of complex Fourier series

$$V(\mathbf{r}) = \sum_{\mathbf{K}} U_{\mathbf{K}} e^{i\mathbf{K}\cdot\mathbf{r}}, \text{ where } U_{\mathbf{K}} = \frac{1}{a^2c} \int V(\mathbf{r}) e^{-i\mathbf{K}\cdot\mathbf{r}} d\mathbf{r}. \quad (\text{A4})$$

Similarly for the reciprocal effective mass

$$\frac{1}{m^*(\mathbf{r})} = \sum_{\mathbf{K}} M_{\mathbf{K}} e^{i\mathbf{K}\cdot\mathbf{r}}, \text{ where } M_{\mathbf{K}} = \frac{1}{a^2c} \int \frac{1}{m^*(\mathbf{r})} e^{-i\mathbf{K}\cdot\mathbf{r}} d\mathbf{r}. \quad (\text{A5})$$

Where the integrations are carried out within the unit cell  $a \times a \times c$ .

Equation (A2) has three multiplication terms that involve Fourier series. The products can be rearranged and simplified as

$$\frac{1}{m^*(\mathbf{r})} \nabla^2 \Psi(\mathbf{r}) = - \sum_{\mathbf{q}} e^{i\mathbf{q}\cdot\mathbf{r}} \left[ \sum_{\mathbf{K}'} M_{\mathbf{K}-\mathbf{K}'} C_{\mathbf{k}+\mathbf{K}'} (\mathbf{k} + \mathbf{K}')^2 \right], \quad (\text{A6})$$

$$\begin{aligned} \nabla \cdot \frac{1}{m^*(\mathbf{r})} \nabla \Psi(\mathbf{r}) \\ = - \sum_{\mathbf{q}} e^{i\mathbf{q}\cdot\mathbf{r}} \left[ \sum_{\mathbf{K}'} M_{\mathbf{K}-\mathbf{K}'} C_{\mathbf{k}+\mathbf{K}'} (\mathbf{K} - \mathbf{K}') \cdot (\mathbf{k} + \mathbf{K}') \right], \end{aligned} \quad (\text{A7})$$

$$V(\mathbf{r})\Psi(\mathbf{r}) = \sum_{\mathbf{q}} e^{i\mathbf{q}\cdot\mathbf{r}} \left( \sum_{\mathbf{K}'} U_{\mathbf{K}-\mathbf{K}'} C_{\mathbf{k}+\mathbf{K}'} \right), \quad (\text{A8})$$

where  $\mathbf{q}=\mathbf{k}+\mathbf{K}$ .

Putting them to the BenDaniel-Duke's equation in Eq. (A2), we now have

$$\sum_{\mathbf{q}} e^{i\mathbf{q}\cdot\mathbf{r}} \sum_{\mathbf{K}'} \left\{ \frac{\hbar^2}{2} M_{\mathbf{K}-\mathbf{K}'} [(\mathbf{k}+\mathbf{K}')^2 + (\mathbf{K}-\mathbf{K}') \cdot (\mathbf{k}+\mathbf{K}')] - \delta_{\mathbf{K}-\mathbf{K}'} E + U_{\mathbf{K}-\mathbf{K}'} \right\} C_{\mathbf{k}+\mathbf{K}'} = 0. \quad (\text{A9})$$

With  $\sum_{\mathbf{q}} e^{i\mathbf{q}\cdot\mathbf{r}}=0$  as the trivial solution, now we arrive at the secular equation of the Hamiltonian

$$\sum_{\mathbf{K}'} \left\{ \frac{\hbar^2}{2} M_{\mathbf{K}-\mathbf{K}'} [(\mathbf{k}+\mathbf{K}')^2 + (\mathbf{K}-\mathbf{K}') \cdot (\mathbf{k}+\mathbf{K}')] - \delta_{\mathbf{K}-\mathbf{K}'} E + U_{\mathbf{K}-\mathbf{K}'} \right\} C_{\mathbf{k}+\mathbf{K}'} = 0. \quad (\text{A10})$$

If the carriers' effective mass is isotropic in real space, the Fourier expansion of the reciprocal effective mass has only a single component:  $M_{\mathbf{K}}=(1/m^*)\delta_{\mathbf{K}}$ , thus Eq. (A10) reduces to the familiar Schrödinger's equation in momentum space

$$\left[ \frac{\hbar^2}{2m^*} (\mathbf{k}+\mathbf{K})^2 - E \right] C_{\mathbf{k}+\mathbf{K}} + \sum_{\mathbf{K}'} U_{\mathbf{K}-\mathbf{K}'} C_{\mathbf{k}+\mathbf{K}'} = 0. \quad (\text{A11})$$

\*Author to whom correspondence should be addressed. Mailing address: Center for Optical Technologies, Lehigh University, Sinclair Laboratory, Room 226, 7 Asa Drive, Bethlehem, PA 18015, USA. Email address: bsooi@lehigh.edu

<sup>1</sup>L. Goldstein, F. Glas, J. Y. Marzin, M. N. Charasse, and G. Leroux, *Appl. Phys. Lett.* **47**, 1099 (1985).

<sup>2</sup>D. Leonard, M. Krishnamurthy, C. M. Reaves, S. P. Denbaars, and P. M. Petroff, *Appl. Phys. Lett.* **63**, 3203 (1993).

<sup>3</sup>D. Bimberg, N. N. Ledentsov, M. Grundmann, N. Kirstaedter, O. G. Schmidt, M. H. Mao, V. M. Ustinov, A. Y. Egorov, A. E. Zhukov, P. S. Kopev, Zh. I. Alferov, S. S. Ruvimov, U. Gosele, and J. Heydenreich, *Jpn. J. Appl. Phys., Part 1* **35**, 1311 (1996).

<sup>4</sup>R. Leon, Y. Kim, C. Jagadish, J. Zou, and D. J. H. Cockayne, *Appl. Phys. Lett.* **69**, 1888 (1996).

<sup>5</sup>R. Leon, S. Fafard, P. G. Piva, S. Ruvimov, and Z. Liliental-Weber, *Phys. Rev. B* **58**, R4262 (1998).

<sup>6</sup>N. Holonyak, Jr., *IEEE J. Sel. Top. Quantum Electron.* **4**, 584 (1998). For a comprehensive review see, E. H. Li, in *Semiconductor Quantum Wells Intermixing*, (Gordon and Breach Science, Amsterdam, 2000).

<sup>7</sup>S. Malik, C. Roberts, R. Murray, and M. Pate, *Appl. Phys. Lett.* **71**, 1987 (1997).

<sup>8</sup>C. Lobo, R. Leon, S. Fafard, and P. G. Piva, *Appl. Phys. Lett.* **72**, 2850 (1998).

<sup>9</sup>R. Leon and S. Fafard, *Phys. Rev. B* **58**, R1726 (1998).

<sup>10</sup>S. S. Li and J. B. Xia, *J. Appl. Phys.* **84**, 3710 (1998).

<sup>11</sup>S. J. Xu, X. C. Wang, S. J. Chua, C. H. Wang, W. J. Fan, J. Jiang, and X. G. Xie, *Appl. Phys. Lett.* **72**, 3335 (1998).

<sup>12</sup>X. C. Wang, S. J. Xu, S. J. Chua, Z. H. Zhang, W. J. Fan, C. H. Wang, J. Jiang, and X. G. Xie, *J. Appl. Phys.* **86**, 2687 (1999).

<sup>13</sup>J. J. Dubowski, C. N. Allen, and S. Fafard, *Appl. Phys. Lett.* **77**, 3583 (2000).

<sup>14</sup>Y. Ji, W. Lu, G. Chen, X. Chen, and Q. Wang, *J. Appl. Phys.* **93**, 1208 (2003).

<sup>15</sup>S. Fafard and C. N. Allen, *Appl. Phys. Lett.* **75**, 2374 (1999).

<sup>16</sup>J. H. Marsh, D. Bhattacharyya, A. S. Helmy, E. A. Avrutin, and A. C. Bryce, *Physica E (Amsterdam)* **8**, 154 (2000).

<sup>17</sup>N. Perret, D. Morris, L. Franchomme-Fosse, and R. Cote, S. Fafard, V. Aimez, and J. Beauvais, *Phys. Rev. B* **62**, 5092 (2000).

<sup>18</sup>F. E. Prins, S. Y. Nikitin, G. Lehr, H. Schweizer, and G. W.

Smith, *Phys. Rev. B* **49**, 8109 (1994).

<sup>19</sup>C. Pryor, M.-E. Pistol, and L. Samuelson, *Phys. Rev. B* **56**, 10404 (1997).

<sup>20</sup>C. Pryor, *Phys. Rev. B* **57**, 7190 (1998).

<sup>21</sup>O. Stier, M. Grundmann, and D. Bimberg, *Phys. Rev. B* **59**, 5688 (1999).

<sup>22</sup>M. A. Cusack, P. R. Briddon, and M. Jaros, *Phys. Rev. B* **56**, 4047 (1997).

<sup>23</sup>M. Califano and P. Harrison, *Phys. Rev. B* **61**, 10959 (2000).

<sup>24</sup>M. Roy and P. A. Maksym, *Phys. Rev. B* **68**, 235308 (2003).

<sup>25</sup>D. J. BenDaniel and C. B. Duke, *Phys. Rev.* **152**, 683 (1966).

<sup>26</sup>M. A. Cusack, P. R. Briddon, and M. Jaros, *Phys. Rev. B* **54**, R2300 (1996).

<sup>27</sup>M. Grundmann, O. Stier, and D. Bimberg, *Phys. Rev. B* **52**, 11969 (1995).

<sup>28</sup>M. Califano and P. Harrison, *J. Appl. Phys.* **88**, 5870 (2000).

<sup>29</sup>To avoid division by zero, one could use an approximation of a very small number ( $\epsilon \sim 1 \times 10^{-6}$ ) for zero  $n$ ,  $m$ , or  $l$  indexes and for pyramidal FCs the following identity can be used:  $\cos(\phi - i \tanh^{-1} a/b) = b \cos \phi - ia \sin \phi$ .

<sup>30</sup>Complete pyramid and cubic QD are special cases of truncated pyramid from which their FCs can be derived. For cubic QD:  $d=h=b$ , and complete pyramid QD:  $d=0$ .

<sup>31</sup>D. M. Bruls, J. W. A. M. Vugs, P. M. Koenraad, H. W. M. Salemink, J. H. Wolter, M. Hopkinson, M. S. Skolnick, Fei Long, and S. P. A. Gill, *Appl. Phys. Lett.* **81**, 1708 (2002).

<sup>32</sup>Caution should be taken when modelling WL in interdiffused QD system. Unless the WLs are really closely spaced, the unit cell lattice constant  $c$  should be sufficiently large so that the WL does not represent a significant fraction of the unit cell, for otherwise it will yield erroneously lower bound state energies at high diffusion length.

<sup>33</sup>S. W. Ryu, I. Kim, B. D. Choe, and W. G. Jeong, *Appl. Phys. Lett.* **67**, 1417 (1995).

<sup>34</sup>W. P. Gillin, *J. Appl. Phys.* **85**, 790 (1999).

<sup>35</sup>The choice of  $R=\sqrt[3]{4V_{QD}/3\pi}$  to represent the size of QD is motivated by the spherical resemblance of the probability density isosurface of the ground state wave functions.

<sup>36</sup>We do not consider lens-shaped or pyramidal QDs with aspect ratio  $h/b>0.5$  as they are not practically relevant.